On the transformation temperatures of Ti-6Al-4V: Effect of oxygen pick-up during Laser Powder Bed Fusion

Quentin Gaillard, X Boulnat, Sophie Cazottes, Sylvain Dancette, Christophe Desrayaud

On the transformation temperatures of Ti-6Al-4V: effect of oxygen pick-up during Laser Powder Bed Fusion

Quentin Gaillard [a,b,*], Xavier Boulnat [b], Sophie Cazottes [b], Sylvain Dancette [b,c], Christophe Desrayaud [a]

[a] *Mines Saint-Etienne, Univ Lyon, CNRS, UMR 5307 LGF, F-42023 Saint-Etienne, France*

[b] *Université de Lyon, INSA Lyon, MATEIS, UMR CNRS 5510, F-69621 Villeurbanne, France*

[c] *ElyTMaX IRL3757, CNRS, Université de Lyon, INSA Lyon, Centrale Lyon, Université Claude Bernard Lyon 1, Tohoku University, Sendai, 980-8577, Japan*

∗ *Corresponding author: quentin.gaillard@emse.fr*

Keywords:

Titanium, Ti-6Al-4V, additive manufacturing, L-PBF, heat treatments, transformation temperatures, X-Ray Diffraction, Differential Scanning Calorimetry

Abstract

Ti-6Al-4V (Ti64) parts manufactured by Laser Powder Bed Fusion (L-PBF) exhibit a fine martensitic microstructure and significant residual stresses that are detrimental for their mechanical performance. Consequently, post-processing heat treatments are necessary to relieve these internal stresses and achieve a microstructure adequate for the mechanical requirements. Given the variations in powder compositions and processing parameters, there is a large scattering of physical properties of both as-built and heat-treated parts. In this context, this study quantifies the link between interstitial contents (specifically, oxygen, nitrogen) and the transition temperatures of as-built parts, using as-atomized pre-alloyed powders for reference. The martensite decomposition temperature and beta transus temperature are assessed using high-temperature X-Ray diffraction and differential scanning calorimetry for both the powder and as-built parts. It was found that the martensite that composes the as-built microstructure can be decomposed into a stable $\alpha + \beta$ structure at temperatures exceeding 490 °C. Oxygen and nitrogen pick-up occurs during the L-PBF process, leading to an elevated beta transus temperature in as-built parts relative to the original powder. This insight provides a guide for optimizing post-processing heat treatments for Ti64 as-built components.

1 Introduction

Research and development in additive manufacturing of metallic materials recently achieved a high degree of technological maturity. Laser powder bed fusion (L-PBF) in particular is now capable of producing dense and functional metallic parts of high geometrical complexity which are of great interest for many applications.

The two-phase Ti-6Al-4V (Ti64) titanium alloy is a widely used structural material in the aerospace industry due to its excellent specific strength and corrosion resistance. When elaborated with conventional processing techniques such as forging and annealing, Ti64 shows a microstructure consisting of both the α (hexagonal close-packed) and β (body-centered cubic) equilibrium phases at room temperature. When the thermo-mechanical manufacturing routine of the material is properly fixed, this stable microstructure implies a good combination of strength and ductility [1, 2]. In contrast, the high cooling rates involved during L-PBF processing of Ti64 create a microstructure consisting of very fine needles of an α' martensitic phase [3, 4]. Significant thermal gradients are also generated during the building process and, as a consequence, large residual stresses develop in the parts as layers are consecutively built [5]. These characteristics result in typical tensile properties of L-PBF Ti64 parts that show a high yield stress and tensile strength but a low ductility compared to the wrought material taken as a reference [4, 6].

To relieve the residual stresses of the as-built parts and achieve a microstructural evolution that helps to balance the static properties of the material, the use of post-processing heat treatments is a topic of main interest for industrial applications. It has been shown in previous studies that post-processing heat treatments performed in the sub-transus range of the alloy (below beta transus temperature) lead to the transformation of the fine α' needles to a coarser mixture of α and β phases [4, 6–8]. It is therefore of great interest to determine the Martensitic Decomposition Temperature (MDT) above which this phase transformation occurs.

In addition, when designing heat-treatments of titanium alloys, a crucial technological parameter to consider is the Beta Transus Temperature (BTT) above which the $\alpha + \beta$ stability domain changes into 100 % of β phase. It is in fact known that exceeding the BTT during heat treatment of Ti64 alloy leads to a drastic β grains growth [9, 10] and possible microstructural heterogeneity due to the cooling rate dependence of the phase transformations from the β domain, followed by mechanical properties deterioration [7, 8]. Based on information dispensed by manufacturers, the BTT for ASTM grade 5 Ti64 ranges between 980 °C and 1 000 °C. As the BTT is dependent on the chemical composition of the alloy [11], these values may vary. In particular, oxygen, nitrogen and carbon are α-forming interstitial elements that increase the BTT significantly: Kahveci and Welsch found in fact that the BTT is raised by 243 °C by 1 wt% of oxygen equivalent [12]. This effect can be therefore drastic in Ti64 powders, where BTT can be as high as 1 200 °C when oxygen is not properly controlled [13]. Regarding the L-PBF process, the

BTT is very likely to be underestimated with the use of powders chemical composition as it is demonstrated that oxygen and nitrogen pick-up occur during samples fabrication in the atmosphere-controlled chamber of the machine [14, 15].
Thus, the object of the present work is to propose an experimental estimation of the transition temperatures (MDT, BTT) of interest for designing post L-PBF process heat treatments of Ti64. The investigations are conducted on as-built parts and on as-atomized pre-alloyed powders as a reference. Then, the effects of oxygen and nitrogen pick-up during the process are discussed.

2 Materials and methods

In the present work, a batch of plasma atomized pre-alloyed Ti64 powder manufactured by Tekna Advanced Materials Inc., Canada, was used. The chemical composition is detailed in Table 1.

Ti	Al	V	Fe	O	C	N	H
Base	6.22	3.87	0.18	0.14	0.009	0.02	0.004

Table 1: Chemical composition (wt%) of the batch of grade 5 Ti64 powder provided by the supplier.

Figure 1.a shows that most of the powder particles have a spherical shape and some of them exhibit a few attached satellites whose size is below 5 µm. Figure 1.b indicates the particle size distribution of the powder batch measured by laser diffraction using a Malvern Panalytical Mastersizer 3000 equipped with a dry dispersion unit. D(10), D(50) and D(90) are 6.9 µm, 13.8 µm and 21.9 µm respectively.

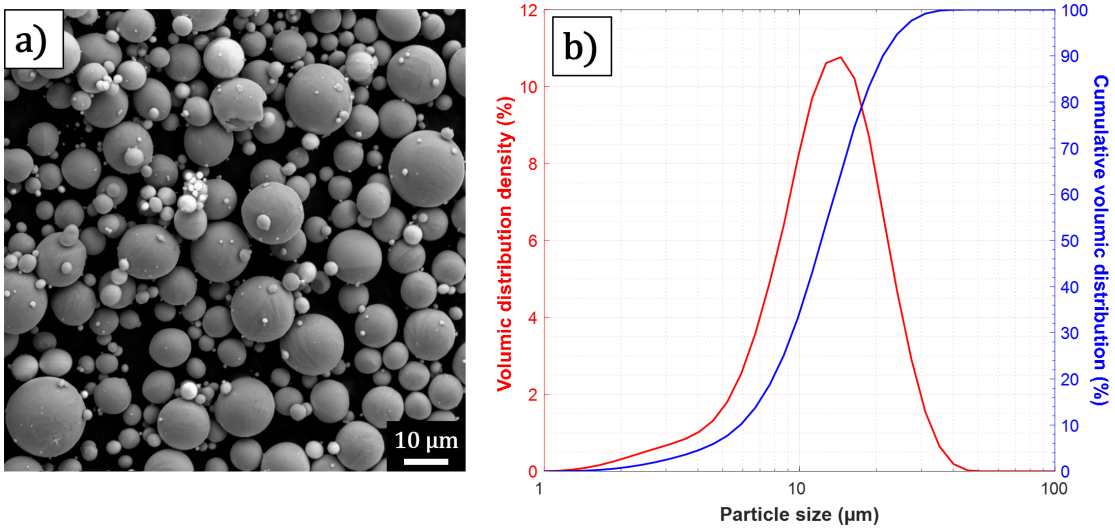

Figure 1: Secondary electron SEM image (a) and volumic particle size distribution (b) of the plasma atomized Ti64 powder batch used.

Samples were built with the studied powder batch using a FormUp 350 L-PBF machine provided by AddUp, France. The fabrication step was performed under an argon protective atmosphere with an oxygen concentration measured at the top of the chamber lower than 500 ppm. The orientations of the parts are described using the axis of the L-PBF machine with Z axis being the building direction.

Oxygen (O) and nitrogen (N) concentrations before (powder) and after (as-printed part) building was determined through an inert gas fusion method using a LECO device. To ensure the reproducibility of the technique, 5 measurements were made on 100 mg samples. As-printed samples were extracted in the bulk of a *post mortem* Charpy impact V-notch specimen constructed near-net shape along the Z-axis. The impact properties of the as-printed material, as well as those after various sub-transus heat treatments, are detailed in Ref. [16]. Examinations of the microstructure by X-Ray Diffraction (XRD) and scanning electron microscopy (SEM) were made on 3 mm thick pieces cut from 15 mm^3 cubic samples. Sample preparation was conducted by grinding the pieces with SiC paper up to 320 grit size followed by 9 µm diamond solution and chemical-mechanical polishing with a mixture of colloidal silica, hydrogen peroxide and ammonia. A vibratory polishing step with colloidal silica was applied before taking the SEM pictures in backscattered electron mode. Micrographs were also taken on an Olympus GX51 equipped with a motorized stage after etching of the samples for 90 s with Kroll reagent. To determine a first estimation of the MDT, high temperature XRD was performed on a Bruker D8 advance diffractometer equipped with a Ni K_β filter, a Lynxeye XE detector and a Cu-K_α ($\lambda = 1.54$ Å) X-Ray tube source operating at 40 kV and 40 mA. Heating of the sample occurred in an Anton Paar HTK 1200N sample stage furnace capable of producing homogeneous temperature up to 1 200 °C by radiation. Secondary vacuum (10^{-3} mbar) was reached by use of a Pfeiffer Vacuum HiCube 80 pumping station.

In this study, Differential Scanning Calorimetry (DSC) was chosen to determine the transition temperatures as this technique is characterized by high sensitivity to thermal effects induced by phase transformations [17, 18]. DSC investigations were carried out on a SETARAM Labsys Evo calorimeter equipped with a high sensitivity 3D-Cp sensor especially designed to detect low intensity thermal effects. All DSC experiments were performed in Al_2O_3 crucibles with an empty crucible taken as a reference. The experiments were conducted under an argon of commercial purity (Ar $\geq$ 99.999 %). After pumping the working chamber three times to a vacuum level of 20 mbar, the argon flow is set to (50 mL min^{-1}). The as-printed samples used for DSC were extracted in the bulk of the same Charpy impact V-notch specimen used for chemical composition analysis. When preparing the samples, attention was paid to fill at best the volume of the crucible with material in order to increase the magnitude of the DSC signal.

3 Results and Discussion

The oxygen (O) and nitrogen (N) concentrations in the Ti64 powder and in as-built parts determined by inert gas fusion method are available in Table 2. From these results, it is found that Ti64 absorbs O during printing of the parts ($\approx +200$ ppm). A little N pick-up also tends to occur even if it appeared to be less distinct than oxygen pick-up regarding the uncertainties of the concentrations measured in this study.

Ti64 state	O mass content (ppm)	N mass content (ppm)
As-atomized powder	$1\,529 \pm 23$	168 ± 30
As-built part	$1\,698 \pm 30$	240 ± 43

Table 2: O/N chemical composition in the Ti64 powder and as-built parts.

Microstructural investigations reveal that both the powder and the as-built part consist of an acicular α' microstructure with the presence of very thin and entangled needles. These structures are inherited from the very fast cooling rates from the β domain occurring during both processes with an order of magnitude of 10^3 K s^{-1} for plasma atomization [19] and 10^4 K s^{-1} for laser melting of powders [20]. From Fig 2.a and 2.b, it can be observed that some martensitic needles contain a multitude of twins. The presence of twins inside the α lamellae is typical from the α' phase as they contribute to accommodate and release stresses of the martensitic transformation [3, 4]. According to these observations, it is expected that martensitic decomposition could take place in both the powder and the as-built parts leading to a possible estimation of the MDT.

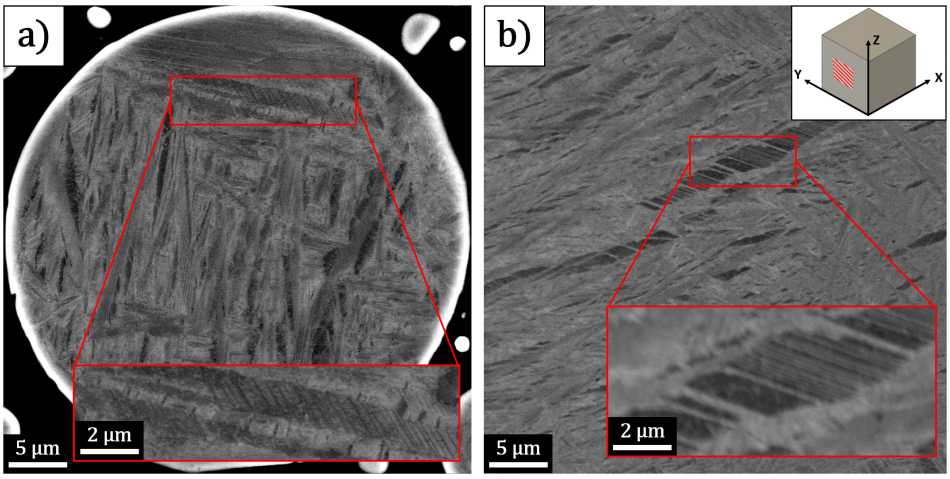

Figure 2: Backscattered electron SEM images showing the acicular microstructure of a powder particle (a) and of an as-built Ti64 cube (b). The high magnification inserts denote that some of the martensitic needles contain a multitude of twins.

To determine a first estimation of the MDT, high temperature XRD was carried out on a thin sample cut and polished in the XZ plane of an as-printed cube. For time saving purposes, XRD acquisitions were only made in a low diffraction angles range. Before high temperature measurements, a first scan was done at 30 °C to have a reference before heating up to 500 °C. From 500 °C to 800 °C, heating with a step size of 5 °C followed by a XRD scan was set. At each step, a timeout of 120 s was applied before XRD measurements to reach equilibrium.

In the purpose to clarify the results, figure 3.a only shows the XRD spectra between 500 °C and 800 °C with a step size of 50 °C. As temperature rises, the peaks are shifted to lower angular values, highlighting an increase of lattice parameters due to thermal expansion [21, 22]. Peaks identification has been performed with MAUD software and the corresponding crystal planes are indicated in figure 3.a. Zoom window (figure 3.b) reveals a $(110)_\beta$ peak starting from 600 °C which is not visible on the curves at lower temperature. The detection of this peak indicates that α' started to decompose into a mixture of $\alpha+\beta$ during the experiment. The $(110)_\beta$ peak was distinctively seen starting from the 565 °C XRD spectra. This gives a first estimation of the MDT using this setup. It can be noticed on 3.b that the intensity of the $(110)_\beta$ peak increases until reaching a maximum around 650 °C, indicating an increase of the diffracting volume of β phase. The intensity decreases at 700 °C and the peak is not anymore visible at 750 °C and 800 °C. This observation is likely due to the activation of oxygen diffusion with temperature as the sample became very colored after the experiment (see figures 4.b and 4.c). Oxygen is indeed an α-forming element so the more oxygen diffuses into the metal, the less the stability of β phase. Estimated X-Ray penetration depth in titanium with a copper source is about 5-6 µm [23]. Thus, XRD measurements at temperatures where oxygen is highly diffusive in titanium probably took place in the oxygen-enriched layer, pointed out as alpha-case in several references [16, 24, 25] and visible in Fig. 4.d after chemical attack with Weck's reagent (NH_4HF_2 dissolved in ethanol and water).

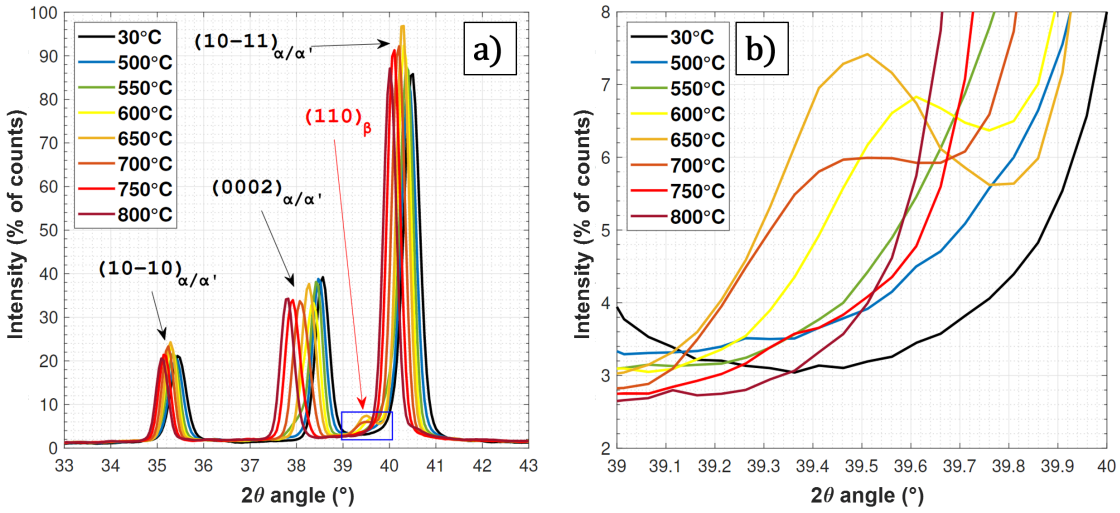

Figure 3: XRD spectra of Ti64 as-built part at various temperatures (a) and corresponding blue frame zoom on the β (100) peak (b).

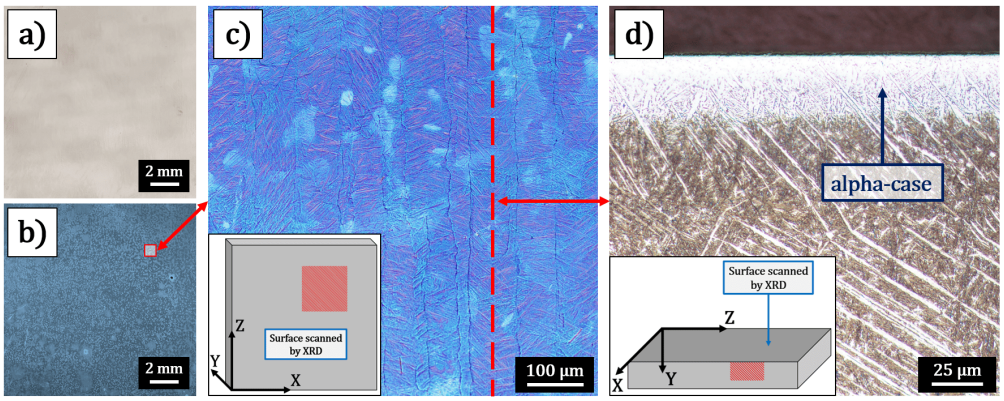

Figure 4: (a) Pictures of the sample's surface before and (b,c) after *in situ* XRD thermal cycle. (d) Transverse cross section of the post-XRD sample revealing an alpha-case layer below the probed surface.

For all the DSC analyses, the thermal cycle consisted in heating from 40 °C to 1 200 °C followed by a 10 min isothermal exposure followed by cooling from 1 200 °C to 40 °C. The cycle was applied twice consecutively on each sample. Heating and cooling rates are crucial parameters to consider in thermal analysis: low heating rates lead to a considerable decrease of thermal peak intensity and high cooling rates result in inhomogeneity between furnace temperature and sample temperature [17, 26]. For this research, heating and cooling rates were fixed at 20 K min^{-1}, as it appeared to be a good compromise with this device. It is known that when an endothermic or an exothermic peak is detected by use of thermal analysis during continuous heating, the corresponding phase transformation always begins and ends later than in equilibrium conditions (when heating rate is nil). Hence, the extremum point does not correspond to the beginning or the end of the phase transformation of interest. To avoid this, some authors use the extremum of the first-time derivative of the heat flow versus temperature to determine a value corresponding to the starting or the finishing temperature of a phase transformation occurring during continuous heating [18, 27]. This approach was used to estimate the MDT and BTT in this study. The DSC-curves (heat flow in W g^{-1}) and D-DSC curves (heat flow derivative in W g^{-1} K^{-1}) during continuous heating are presented in figure 5.a for powder and in figure 5.b for as-built part. It can be seen on both graphs that an exothermic peak is visible around 500 °C during first heating while second heating resulted in no exothermic peak. As shown in figures 6.a and 6.b, the microstructure of the as-built part changed from acicular α' needles in columnar parent β grains to equilibrium $\alpha + \beta$ with α-Widmanstätten colonies in equiaxial parent β grains. This indicates that the exothermic peaks were associated to an irreversible metastable phase transformation corresponding to the α' decomposition. The measured MDT are similar for powder and as-built part, respectively 495 °C and 490 °C. It is therefore considered that the stability of the α' phase is equivalent in both cases, leading to a comparable martensitic decomposition kinetic upon heating. These MDT values are however lower than the *in situ* XRD estimation. This result could be explained by the fact that when

the martensite decomposition started, the freshly transformed β phase fraction was too low to give an intensity higher than the detection limit of the XRD device.

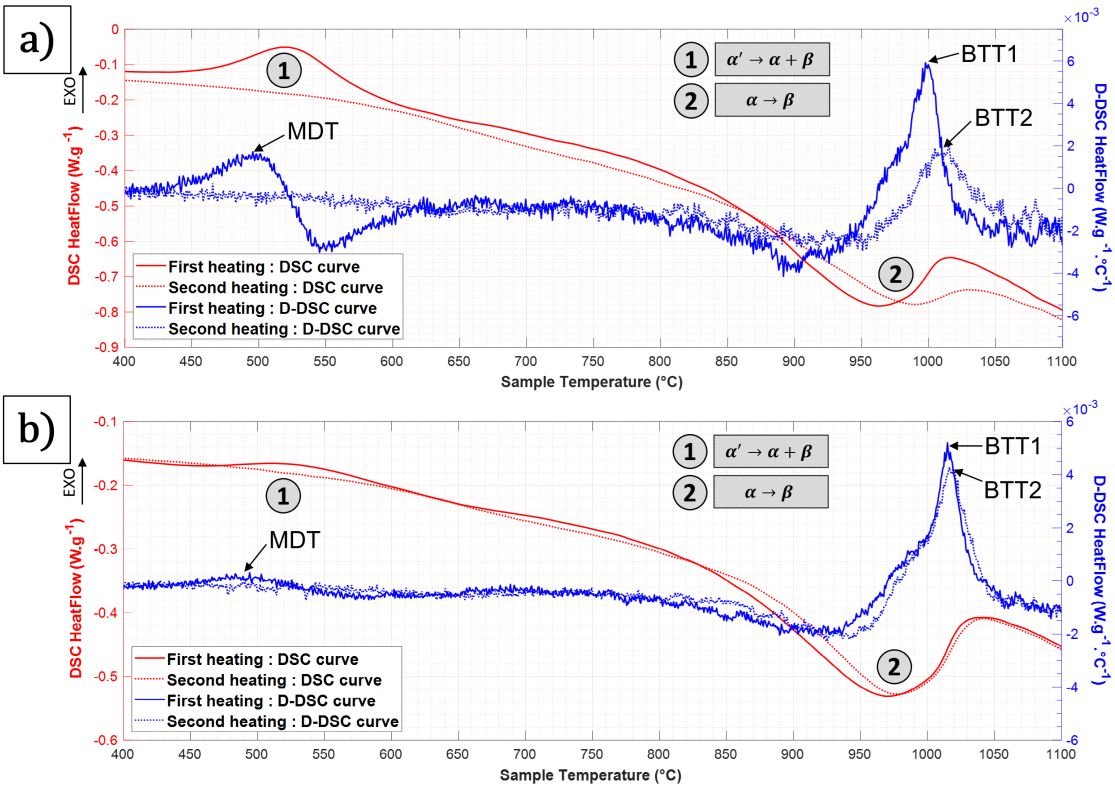

Figure 5: DSC curves of (a) powder and (b) as-built part during continuous heating.

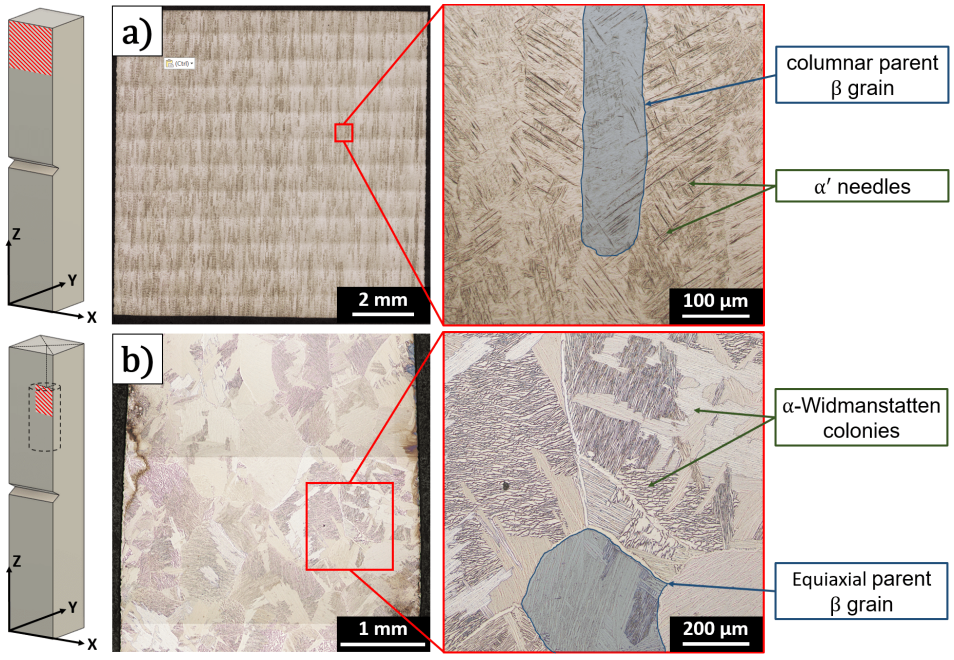

Figure 6: Optical micrographs showing the microstructrure in the XZ plane of (a) an as-built part and (b) on the same part after cooling from 1 200 °C to 40 °C at 20 K min^{-1} in the DSC device.

Figures 5.a and 5.b also show an endothermic peak around 1 000 °C that is present in first and second heating of Ti64 powder and as-built part. These peaks correspond to the beta transus of the alloy and are spread on a wide temperature range. In fact, the kinetics of α to β phase transformation is governed by a dissolution temperature around 700 °C from which the β phase fraction grows exponentially with temperature for slow heating [13, 21, 22]. For comparison with the experimental work, Thermo-Calc calculations were performed with the TCTI4 database. The chemical composition of the simulated alloy was taken from table 1 data, except for oxygen and nitrogen contents that were taken from table 2 for both the powder and the as-built part. Figure 7 depicts the evolution of the equilibrium mole fraction of α and β phases as the function of temperature. From these curves, simulated BTT_{TC} were determined as the temperatures at which the equilibrium α and β phase fractions reaches 0 % and 100 % respectively.

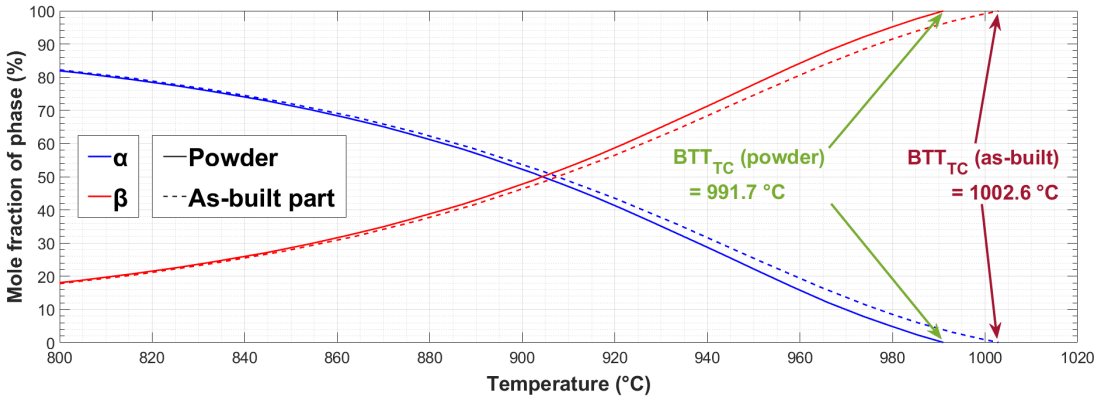

Figure 7: Equilibrium mole fraction of α and β phases as the function of temperature calculated using the TCTI4 database of Thermo-Calc software. The chemical compositions of the powder and the as-built part were taken from tables 1 and 2.

The experimental BTT estimated with DSC for both first and second heating (BTT_1 and BTT_2 repectively) and the simulated BTT_{TC} are compared in figure 8.a. From these results, it can be observed that the BTT_1 and the BTT_{TC} are close for both the powder and the as-built part. This illustrates the reliability of the BTT determination by use of the extremum of the DSC heat flux first time derivative for Ti64 alloy. The gap of +12 °C between the BTT_{TC} and the BTT_1 for the as-built part may be explained by the fact that the higher the heating rate, the lower the system is close to the equilibrium conditions [22]. To measure the impact of the heating rate, two DSC cycles were made with heating rates fixed at 10 K min^{-1} and 40 K min^{-1} on as-built samples similar to the one performed at 20 K min^{-1}. From figure 8.b, it is visible that the heating rate has a strong influence on the BTT estimation and that the gap between the BTT_{TC} and the BTT_1 measured at 10 K min^{-1} is reduced to +4 °C only.

The BTT_1 of the as-built part determined during first continuous heating is +17 °C higher than the BTT_1 of the powder. It is therefore noticeable that this increase is correlated to the oxygen and nitrogen pick-up during the L-PBF process. Similar con-

clusions are dressed from the Thermo-Calc simulations with a lower deviation (+12 °C) measured between powder and as-built part with different O/N concentrations. However, it should be noted that titanium alloys are also sensitive to carbon pick-up when submitted to high temperature manufacturing routines [28, 29]. It was not possible to characterize the carbon content in this study but by imposing an arbitrary [C] concentration of 0.02 wt% (+100 ppm compared to the powder) in the Thermo-Calc simulation, the increase of BTT_{TC} between the powder and the as-built part raises to +16 °C.

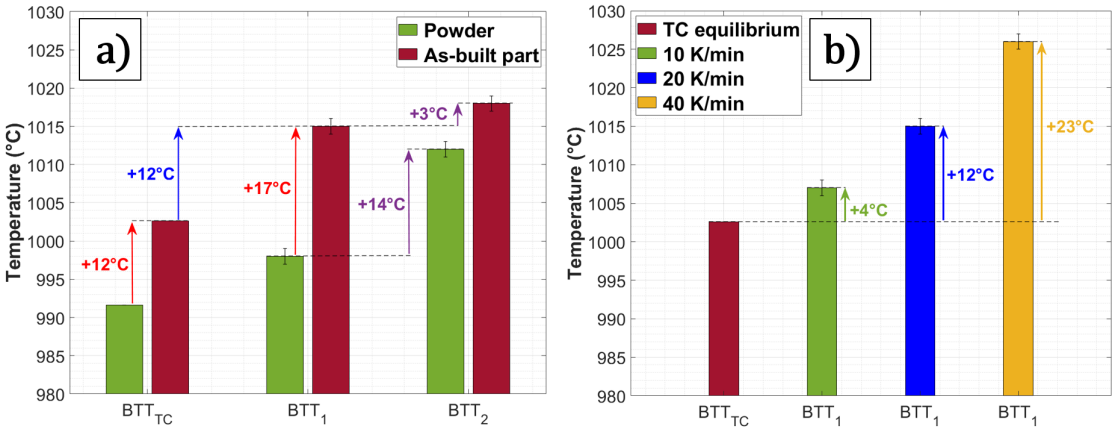

Figure 8: Beta transus temperatures estimated from the DSC scans performed at 20 K min^{-1} on the powder and the as-built part (a). BTT_1 and BTT_2 correspond to first and second heating respectively. BTT_{TC} were taken from figure 7. Beta transus temperatures at first heating (BTT_1) estimated from the DSC scans performed at 10 K min^{-1}, 20 K min^{-1} and 40 K min^{-1} on as-built samples (b).

Finally, figure 9 show that the two DSC thermal cycles up to 1 200 °C performed on the powder sample led to a partial sintering. The resulting powder aggregate was cut in three identical sections and O/N inert gas fusion measurements were made. The results displayed in figure 9 reveal an important increase of the oxygen content, with a gradient from top to bottom that appears to be linked to the direction of the argon flux. This result has to be compared with the difference between the first and the second continuous heating in figure 8.a. Indeed, it can be observed that an important 14 °C increase occurred for the powder while only a 3 °C increase occurred for the as-built part. Specific surface area of the powder sample is very large compared to the as-built fully dense sample used for DSC. Therefore, oxidation and oxygen pick-up in the powder during first heating probably played an important role in increasing the BTT measured during second heating [12]. The high affinity of Ti with interstitial elements makes very difficult the complete protection of samples during DSC as-well-as during high temperature XRD. However, it should be borne in mind that α phase morphology can also have an effect on the shape of the endothermic peak related to the transformation [18, 27].

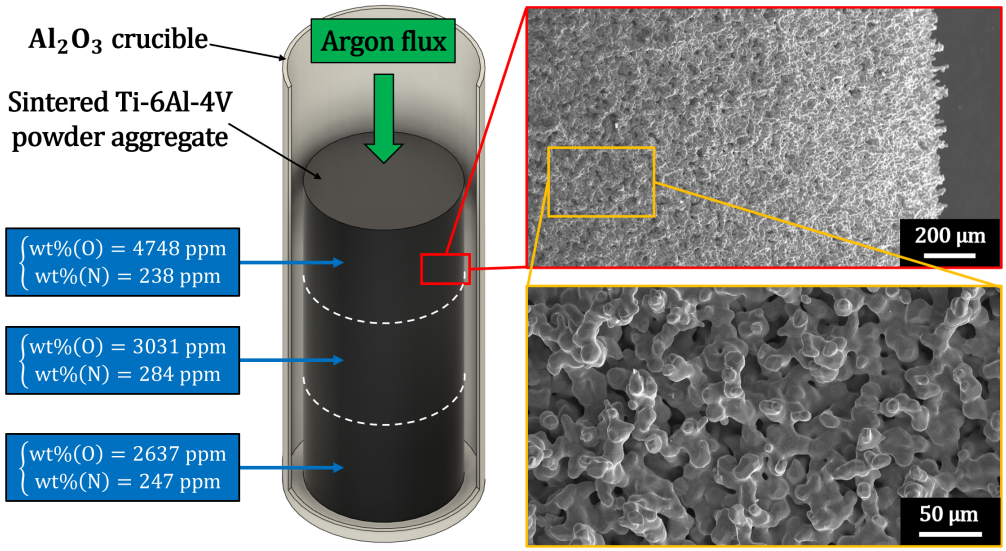

Figure 9: Secondary electron SEM images of the sintered Ti64 powder aggregate after DSC thermal cycle at 20 K min^{-1} and corresponding O/N chemical composition measured in three slices.

4 Conclusions

In this study, experimental measurements of the phase transformations that can occur during the post-processing heat treatment of Ti64 parts, as printed by L-PBF, were performed. These measurements were conducted for both as-printed material and as-atomized pre-alloyed powders as a reference. Notably, DSC investigations were undertaken to gauge the influence of oxygen content on the martensite decomposition temperature (MDT) and the beta transus temperature (BTT). These findings offer insights for devising post-processing heat treatments of Ti64 printed by L-PBF. The following conclusions are drawn from this work:

- The oxygen concentration difference between the powder and the as-printed part sees an average increase of 200 ppm, indicating that oxygen pick-up occurs during the L-PBF process.

- Both the powder and the as-built part exhibit a martensitic microstructure. The metastable α' phase can be decomposed into a mixture of stable $\alpha + \beta$ phases. The MDT was estimated to be 565 °C using the *in situ* high-temperature XRD setup, and 490 °C through DSC analysis. This underscores that martensite can transition into equilibrium phases well below the dissolution temperature, typically cited around 700 °C for the Ti64 alloy.

- The variation in oxygen concentration between the powder and as-built parts results in an estimated increase of +17 °C in the alloy's BTT. In contrast, the estimated MDT appears to remain unaffected by this shift in chemical composition.

Data availability

The raw/processed data required to reproduce these findings cannot be shared at this time as the data also forms part of an ongoing study.

CRediT authorship contribution statement

Quentin Gaillard: Conceptualisation, Writing - Original Draft, Investigation, Visualisation. **Xavier Boulnat**: Conceptualisation, Supervision, Writing - Review & Editing. **Sophie Cazottes**: Conceptualisation, Supervision, Writing - Review & Editing. **Sylvain Dancette**: Conceptualisation, Writing - Review & Editing. **Christophe Desrayaud**: Supervision, Validation, Funding acquisition.

Declaration of Competing Interest

The authors declare that they have no known competing financial interests or personal relationships that could have appeared to influence the work reported in this paper.

Acknowledgments

This work performed at LGF and MATEIS laboratories falls within the framework of the AEROPRINT project supported by the French company Dassault Aviation and the Auvergne-Rhônes-Alpes Region. The authors are grateful for their financial support and especially thank the project team of the Argonay production site for providing the powder and fabricating the samples studied in this work. The authors would like to acknowledge the help of Marie Jansonnet for carrying out the oxygen and nitrogen analysis, Marie-Claude Bertholin for performing the particle size distribution measurements, Sandrine Cardinal for the XRD investigations and Michel Perez for helping with the DSC device.

References

[1] G. Lütjering. "Property Optimization through Microstructural Control in Titanium and Aluminum Alloys". In: *Materials Science and Engineering: A* 263.2 (1999), pp. 117–126. ISSN: 09215093. DOI: 10.1016/S0921-5093(98)01169-1.

[2] S. Semiatin and T. Bieler. "The Effect of Alpha Platelet Thickness on Plastic Flow during Hot Working of TI–6Al–4V with a Transformed Microstructure". In: *Acta Materialia* 49.17 (2001), pp. 3565–3573. ISSN: 13596454. DOI: 10.1016/S1359-6454(01)00236-1.

[3] J. Yang, H. Yu, J. Yin, M. Gao, Z. Wang, and X. Zeng. "Formation and Control of Martensite in Ti-6Al-4V Alloy Produced by Selective Laser Melting". In: *Materials & Design* 108 (2016), pp. 308–318. ISSN: 02641275. DOI: 10.1016/j.matdes.2016.06.117.

[4] S. Cao, R. Chu, X. Zhou, K. Yang, Q. Jia, C. V. S. Lim, A. Huang, and X. Wu. "Role of Martensite Decomposition in Tensile Properties of Selective Laser Melted Ti-6Al-4V". In: *Journal of Alloys and Compounds* 744 (2018), pp. 357–363. ISSN: 09258388. DOI: 10.1016/j.jallcom.2018.02.111.

[5] P. Mercelis and J.-P. Kruth. "Residual Stresses in Selective Laser Sintering and Selective Laser Melting". In: *Rapid Prototyping Journal* 12.5 (2006), pp. 254–265. ISSN: 1355-2546. DOI: 10.1108/13552540610707013.

[6] X. Yan, S. Yin, C. Chen, C. Huang, R. Bolot, R. Lupoi, M. Kuang, W. Ma, C. Coddet, H. Liao, and M. Liu. "Effect of Heat Treatment on the Phase Transformation and Mechanical Properties of Ti6Al4V Fabricated by Selective Laser Melting". In: *Journal of Alloys and Compounds* 764 (2018), pp. 1056–1071. ISSN: 09258388. DOI: 10.1016/j.jallcom.2018.06.076.

[7] B. Vrancken, L. Thijs, J.-P. Kruth, and J. Van Humbeeck. "Heat Treatment of Ti6Al4V Produced by Selective Laser Melting: Microstructure and Mechanical Properties". In: *Journal of Alloys and Compounds* 541 (2012), pp. 177–185. ISSN: 09258388. DOI: 10.1016/j.jallcom.2012.07.022.

[8] C. V. Funch, A. Palmas, K. Somlo, E. H. Valente, X. Cheng, K. Poulios, M. Villa, M. A. Somers, and T. L. Christiansen. "Targeted Heat Treatment of Additively Manufactured Ti-6Al-4V for Controlled Formation of Bi-lamellar Microstructures". In: *Journal of Materials Science & Technology* 81 (2021), pp. 67–76. ISSN: 10050302. DOI: 10.1016/j.jmst.2021.01.004.

[9] O. Ivasishin, S. Shevchenko, and S. Semiatin. "Effect of Crystallographic Texture on the Isothermal Beta Grain-Growth Kinetics of Ti–6Al–4V". In: *Materials Science and Engineering: A* 332.1-2 (2002), pp. 343–350. ISSN: 09215093. DOI: 10.1016/S0921-5093(01)01755-5.

[10] S. Semiatin, P. Fagin, M. Glavicic, I. Sukonnik, and O. Ivasishin. "Influence on Texture on Beta Grain Growth during Continuous Annealing of Ti–6Al–4V". In: *Materials Science and Engineering: A* 299.1-2 (2001), pp. 225–234. ISSN: 09215093. DOI: 10.1016/S0921-5093(00)01371-X.

[11] Z. Guo, S. Malinov, and W. Sha. "Modelling Beta Transus Temperature of Titanium Alloys Using Artificial Neural Network". In: *Computational Materials Science* 32.1 (2005), pp. 1–12. ISSN: 09270256. DOI: 10.1016/j.commatsci.2004.05.004.

[12] A. Kahveci and G. Welsch. "Effect of Oxygen on the Hardness and Alpha/Beta Phase Ratio of Ti6Al4V Alloy". In: *Scripta Metallurgica* 20.9 (1986), pp. 1287–1290. ISSN: 00369748. DOI: 10.1016/0036-9748(86)90050-5.

[13] M. Pontoreau, M. Coffigniez, V. Trillaud, C. L. Bourlot, J. Lachambre, L. Gremillard, M. Perez, E. Maire, J. Adrien, P. Steyer, T. Douillard, A. King, and X. Boulnat. "In Situ Synchrotron Study of Sintering of Gas-Atomized Ti-6Al-4 V Powders Using Concomitant Micro-Tomography and X-ray Diffraction: Effect of Particle Size and Interstitials on Densification and Phase Transformation Kinetics". In: *Acta Materialia* 246 (2023), p. 118723. ISSN: 13596454. DOI: 10.1016/j.actamat.2023.118723.

[14] B. Vrancken, S. Buls, J.-P. Kruth, and J. Van Humbeeck. "Influence of Preheating and Oxygen Content on Selective Laser Melting of Ti6Al4V". In: *Annual International Conference on Rapid Product Development Association of South Africa*. Vol. 16. Pretoria, South Africa: Proceedings of the 16th RAPDASA Conference, 2015.

[15] K. Dietrich, J. Diller, S. Dubiez-Le Goff, D. Bauer, P. Forêt, and G. Witt. "The Influence of Oxygen on the Chemical Composition and Mechanical Properties of Ti-6Al-4V during Laser Powder Bed

Fusion (L-PBF)". In: *Additive Manufacturing* 32 (2020), p. 100980. ISSN: 22148604. DOI: 10.1016/j.addma.2019.100980.

[16] Q. Gaillard, X. Boulnat, S. Cazottes, S. Dancette, and C. Desrayaud. "Strength/Ductility Trade-off of Laser Powder Bed Fusion Ti-6Al-4V: Synergetic Effect of Alpha-Case Formation and Microstructure Evolution upon Heat Treatments". In: *Additive Manufacturing* (2023), p. 103772. ISSN: 22148604. DOI: 10.1016/j.addma.2023.103772.

[17] S. Vyazovkin, N. Koga, and C. Schick. *Handbook of Thermal Analysis and Calorimetry*. 2nd ed. Amsterdam: Elsevier. ISBN: 978-0-444-64062-8.

[18] D. Gadeev and A. Illarionov. "Determination of Beta-Transus Temperature of Two-Phase Titanium Alloys Using Differential Scanning Calorimetry". In: *Solid State Phenomena* 284 (2018), pp. 259–264. ISSN: 1662-9779. DOI: 10.4028/www.scientific.net/SSP.284.259.

[19] A. Birt, V. Champagne, R. Sisson, and D. Apelian. "Microstructural Analysis of Ti–6Al–4V Powder for Cold Gas Dynamic Spray Applications". In: *Advanced Powder Technology* 26.5 (2015), pp. 1335–1347. ISSN: 09218831. DOI: 10.1016/j.apt.2015.07.008.

[20] T. Vilaro, C. Colin, and J. D. Bartout. "As-Fabricated and Heat-Treated Microstructures of the Ti-6Al-4V Alloy Processed by Selective Laser Melting". In: *Metallurgical and Materials Transactions A* 42.10 (2011), pp. 3190–3199. ISSN: 1073-5623, 1543-1940. DOI: 10.1007/s11661-011-0731-y.

[21] J. Elmer, T. Palmer, S. Babu, and E. Specht. "In Situ Observations of Lattice Expansion and Transformation Rates of α and β Phases in Ti–6Al–4V". In: *Materials Science and Engineering: A* 391.1-2 (2005), pp. 104–113. ISSN: 09215093. DOI: 10.1016/j.msea.2004.08.084.

[22] Y. Lakroune, D. Connétable, J. Hugues, P. Hermantier, P. Barriobero-Vila, and M. Dehmas. "Microstructural Evolution during Post Heat Treatment of the Ti–6Al–4V Alloy Manufactured by Laser Powder Bed Fusion". In: *Journal of Materials Research and Technology* 23 (2023), pp. 1980–1994. ISSN: 22387854. DOI: 10.1016/j.jmrt.2023.01.123.

[23] V. Hauk and H. Behnken. *Structural and Residual Stress Analysis by Nondestructive Methods: Evaluation, Application, Assessment*. Amsterdam ; New York: Elsevier, 1997. ISBN: 978-0-444-82476-9.

[24] R. Gaddam, B. Sefer, R. Pederson, and M.-L. Antti. "Study of Alpha-Case Depth in Ti-6Al-2Sn-4Zr-2Mo and Ti-6Al-4V". In: *IOP Conference Series: Materials Science and Engineering* 48 (2013), p. 012002. ISSN: 1757-8981, 1757-899X. DOI: 10.1088/1757-899X/48/1/012002.

[25] P. Seth, J. S. Jha, A. Alankar, and S. K. Mishra. "Alpha-Case Formation in Ti–6Al–4V in a Different Oxidizing Environment and Its Effect on Tensile and Fatigue Crack Growth Behavior". In: *Oxidation of Metals* 97.1-2 (2022), pp. 77–95. ISSN: 0030-770X, 1573-4889. DOI: 10.1007/s11085-021-10079-y.

[26] S. Malinov, Z. Guo, W. Sha, and A. Wilson. "Differential Scanning Calorimetry Study and Computer Modeling of $\beta \Rightarrow \alpha$ Phase Transformation in a Ti-6Al-4V Alloy". In: *Metallurgical and Materials Transactions A* 32.4 (2001), pp. 879–887. ISSN: 1073-5623, 1543-1940. DOI: 10.1007/s11661-001-0345-x.

[27] Y. T. Zhu, J. H. Devletian, and A. Manthiram. "Application of Differential Thermal Analysis to Solid-Solid Transitions in Phase Diagram Determination". In: *Journal of Phase Equilibria* 15.1 (1994), pp. 37–41. ISSN: 1054-9714. DOI: 10.1007/BF02667680.

[28] H. Ogden and R. Jaffee. *The Effects of Carbon, Oxygen, and Nitrogen on the Mechanical Properties of Titanium and Titanium Alloys*. Tech. rep. TML-20, 4370612. 1955, TML–20, 4370612. DOI: 10.2172/4370612.

[29] W. L. Finlay and J. A. Snyder. "Effects of Three Interstitial Solutes (Nitrogen, Oxygen, and Carbon) on the Mechanical Properties of High-Purity, Alpha Titanium". In: *JOM* 2.2 (1950), pp. 277–286. ISSN: 1047-4838, 1543-1851. DOI: 10.1007/BF03399001.